

# Nonlinear Regression Models for Determination of Nicotinamide Adenine Dinucleotide Content in Human Embryonic Stem Cells

Anton Salykin · Petr Kuzmic · Olga Kyrylenko ·  
Jindra Musilova · Zdenek Glatz · Petr Dvorak ·  
Sergiy Kyrylenko

Published online: 6 July 2013  
© Springer Science+Business Media New York 2013

**Abstract** Recent evidence suggests that energy metabolism contributes to molecular mechanisms controlling stem cell identity. For example, human embryonic stem cells (hESCs) receive their metabolic energy mostly via glycolysis rather than mitochondrial oxidative phosphorylation. This suggests a connection of metabolic homeostasis to stemness. Nicotinamide adenine dinucleotide (NAD) is an important cellular redox carrier and a cofactor for various metabolic pathways, including glycolysis. Therefore, accurate determination of NAD cellular levels and

dynamics is of growing importance for understanding the physiology of stem cells. Conventional analytic methods for the determination of metabolite levels rely on linear calibration curves. However, in actual practice many two-enzyme cycling assays, such as the assay systems used in this work, display prominently nonlinear behavior. Here we present a diaphorase/lactate dehydrogenase NAD cycling assay optimized for hESCs, together with a mechanism-based, nonlinear regression models for the determination of  $\text{NAD}^+$ , NADH, and total NAD. We also present experimental data on metabolic homeostasis of hESC under various physiological conditions. We show that  $\text{NAD}^+/\text{NADH}$  ratio varies considerably with time in culture after routine change of medium, while the total NAD content undergoes relatively minor changes. In addition, we show that the  $\text{NAD}^+/\text{NADH}$  ratio, as well as the total NAD levels, vary between stem cells and their differentiated counterparts. Importantly, the  $\text{NAD}^+/\text{NADH}$  ratio was found to be substantially higher in hESC-derived fibroblasts versus hESCs. Overall, our nonlinear mathematical model is applicable to other enzymatic amplification systems.

**Electronic supplementary material** The online version of this article (doi:10.1007/s12015-013-9454-3) contains supplementary material, which is available to authorized users.

A. Salykin · P. Dvorak · S. Kyrylenko (✉)  
Department of Biology, Faculty of Medicine, Masaryk University,  
Building A3, Kamenice 735/5, 625 00 Brno-Bohunice,  
Czech Republic  
e-mail: kyrylenk@med.muni.cz

S. Kyrylenko  
e-mail: kyrylenk@gmail.com

A. Salykin · P. Dvorak  
International Clinical Research Center - Center of Biomolecular  
and Cellular Engineering, St. Anne's University Hospital Brno,  
Brno, Czech Republic

P. Kuzmic  
BioKin Ltd, Watertown, MA, USA

O. Kyrylenko  
A. I. Virtanen Institute, University of Eastern Finland, Kuopio,  
Finland

J. Musilova · Z. Glatz  
Department of Biochemistry, Faculty of Science and Central-  
European Institute of Technology (CEITEC), Masaryk University,  
Brno, Czech Republic

**Keywords** NAD · Human embryonic stem cells ·  
hESC-derived fibroblasts · Enzymatic cycling · Nonlinear  
regression · Biochemical assay

## Abbreviations

ADH	Alcohol dehydrogenase
BSA	Bovine serum albumin
CE	Capillary electrophoresis
hESCs	Human embryonic stem cells
NAD	Nicotinamide adenine dinucleotide
PBS	Phosphate buffer saline
POM1	Sodium polyoxotungstate
RFU	Relative fluorescence units

## Introduction

Recent evidence suggests that cellular energy metabolism plays an important role in the control of stem cell identity [1]. It is widely believed that, in contrast to somatic cells, pluripotent stem cells (PSCs) obtain their energy through glycolysis rather than via oxidative phosphorylation [1, 2]. In turn, the process of glycolysis is dependent on the enzyme cascades which use  $\text{NAD}^+/\text{NADH}$  redox couple to sustain generation of both ATP and intermediates for cellular anabolism [3]. Accordingly, both the levels of  $\text{NAD}^+/\text{NADH}$  and their ratio appear to be plausible indicators of metabolic plasticity of stem cells. In addition, NAD values can be used as a predictive parameter in understanding the mechanisms of various metabolic dysfunctions [4–11]. Consequently, there is an increasing demand for a reliable, easy to perform and affordable biochemical assay to determine NAD values in stem cells and other biological samples.

Traditionally, the analytic determination of NAD levels relies on presumably linear calibration curves [12]. However, in actuality the bioanalytic reactions display inherently nonlinear behavior. To deal with such non-linearity, the conventional approach is to remain within the narrow pseudo-linear experimental range [13], where the analyte concentrations are relatively low. This can be achieved by multiple serial dilutions of the sample. The disadvantage of this approach is that it restricts the experimental setup, requiring special manipulations that inevitably increase the overall uncertainty of the determination, because at very low analyte concentrations there is inevitable loss of the assay sensitivity. Alternatively, other biological laboratories would attempt to deal with inherently nonlinear calibration curves e.g. by quantifying their deviation from the linear regression [14], which has its own limitation as it still appeals to the linear fit. In this paper we present a data-analytic approach that recognizes the inherent nonlinearity in the experimental signal, rather than trying to “linearize” it either by high dilution, or by ignoring the deviations from linearity.

Two-enzyme cycling/chemical amplification systems have been brought to prominence by Lowry et al. [15] many decades ago as tools for exquisitely sensitive quantitation of nucleotides and other co-factors. However, cycling mechanisms can rarely show linear behavior within the practically convenient dynamic ranges. On the other hand, analytical calculation methods traditionally require to operate within the linear sector of the calibration curves. Yet, the need to rely on linear data fitting procedures inevitably placed serious restrictions on the experimental design (for review of the linearity requirements in cycling assays see ref. [16]). This is especially valid for research on stem cells, which often require special reagents and expertise, which in turn increases the difficulties and costs for their cultivation substantially.

In addition, contemporary high-throughput assay formats enabled by multi-well plate readers allow the processing of many samples at once. On the other hand, the relatively low sensitivity of these instruments requires the use of comparatively high concentrations of reagents. Thus, maintaining strict linearity of the cycling/amplification assay is very challenging, and is only possible at relatively narrow concentration ranges.

To offer a solution for this challenge, in this report we present a novel method of kinetic data analysis, which relies on reaction mechanism based mathematical modeling, and which no longer requires strict linearity of the experimental data. Instead, our method utilizes appropriate nonlinear fitting models to analyze intrinsically nonlinear experimental data.

In particular, we use a differential-equation formalism to model the progress of the cycling/amplification reaction over time. In this way, we were able to determine the initial reaction rates in a cycling assay precisely and accurately, even though the reaction progress curves were markedly nonlinear. In our newly proposed method, we subsequently utilize the initial rates of the cycling reaction, in dependence on the known quantity of the nucleotide, to construct a nonlinear calibration curve. Finally, this nonlinear calibration is used to determine the quantity of  $\text{NAD}^+$ ,  $\text{NADH}$ , or total NAD in the unknown samples.

The data analytic procedure proposed here is proven to be reproducible and accurate. It can reliably detect changes in NAD parameters evoked by a treatment with an inhibitor of NAD rescue pathway. We used our methodology to compare the NAD values in different hESC lines versus their differentiated counterparts. We also show that cellular NAD parameters undergo alterations upon routine changes of medium. Our approach could be utilized to analyze experimental data from other types of sensitive two-enzyme cycling/amplification assays. It can be used to meet further analytical challenges in bioassay development and optimization.

## Materials and Methods

**Stem Cell Cultures and Treatments** Human embryonic stem cells (hESC) [17] were grown in monolayer on Matrigel (BD Biosciences) in multi-well plates as described [18]. The hESC-derived fibroblasts were kindly provided by Dr. Rotrekl [19]. Separation of  $\text{NAD}^+$  versus  $\text{NADH}$  was done according to the acid/base extraction principle [20, 21]. Briefly, cells were washed twice with ice-cold PBS and lysed in 200  $\mu\text{l}$  (per well in 24-well plate) of 40 mM NaOH/31  $\mu\text{M}$  nucleotidase inhibitor POM1 (Tocris) on ice. For determination of  $\text{NAD}^+$ , 25  $\mu\text{l}$  of lysate was added to 125  $\mu\text{l}$  40 mM NaOH/200 mM  $\text{Na}_2\text{SO}_4$  and heated for 30 min at 60 °C. For determination of

NADH, 25  $\mu\text{l}$  of lysate was heated for 20 min at 60  $^{\circ}\text{C}$ . For determination of total NAD, samples were kept on ice. FK866 was kindly provided by National Institute of Mental Health's (NIMH) Chemical synthesis and drug supply program, USA. Normalization was done to total protein concentration measured in the non-diluted lysates with DC Protein Assay Kit II (Bio-Rad Laboratories) using protein standards (BSA) dissolved in the cell lysis mixture.

**NAD Standards** A standard commercial aliquot of 20.0 mg  $\beta$ -nicotinamide adenine dinucleotide (Sigma) was dissolved in 603  $\mu\text{l}$  of the acidic buffer (40 mM  $\text{H}_2\text{SO}_4$ , 200 mM  $\text{Na}_2\text{SO}_4$ ) to obtain 50 mM stock solution. Eleven standards were prepared with concentrations 36 nM–36 mM. Standards were diluted 36 fold (5  $\mu\text{l}$  to 180  $\mu\text{l}$  total well volume) to obtain the final concentration in the wells spanning from 1 nM to 1  $\mu\text{M}$ .

**Cycling Assays** Cycling assays were performed in 96-well flat-bottom transparent plates using a multi-well fluorescence plate reader (Beckman Coulter DTX 880 Multimode Detector) in 180  $\mu\text{l}$  (5  $\mu\text{l}$  lysate sample or standard plus 175  $\mu\text{l}$  master mix solution) at 22  $^{\circ}\text{C}$ . The principal scheme of the assay is shown on Fig. 1. The concentrations of each component of the reaction mixtures were optimized and customized for stem cell lysates. The final reaction mixtures contained alcohol dehydrogenase (5.85 U/ml), EtOH (0.12 %), diaphorase (78.6  $\mu\text{U/ml}$ ), riboflavin (1  $\mu\text{M}$ ), resazurin (10  $\mu\text{M}$ ), and BSA (0.1 %). Addition of BSA significantly improved the overall reproducibility. The mixing delay time was approximately 2 min. Resorufin fluorescence was measured with excitation at 535 nm and emission at 595 nm in a dynamic mode every 2 min.

**Purification of Diaphorase** Diaphorase (Sigma) was purified by charcoal using the following protocol: 20  $\mu\text{l}$  of 12 mg/ml diaphorase was mixed with 60  $\mu\text{l}$  2 % charcoal in phosphate buffer (pH 7.0) for 30 min at 37  $^{\circ}\text{C}$  filtered through 0.22  $\mu\text{M}$  filter, aliquoted and stored at  $-20^{\circ}\text{C}$ . Such purification

substantially reduces background from NAD bound to some commercially available preparations of diaphorase [13].

**Capillary Electrophoresis** Capillary electrophoresis was performed by following the protocol described elsewhere [22].

**Data Analysis** All data analyses were performed by using the software package DynaFit [23].

**Robust Nonlinear Fit of Progress Curves** Reaction progress curves (time  $t$  vs fluorescence  $F$ ) were fit to Eq. (1) by using Huber's Mini-Max method for robust regression analysis ([24, 25], see Supplement 2 for the DynaFit script). In Eq. (1),  $F_0$  is the offset (baseline) on the signal axis;  $r_p$  is the molar response coefficient of resorufin; and  $[P]$  is the molar concentration of resorufin at time  $t$ .

$$F(t) = F_0 + r_p[P] \quad (1)$$

Resorufin concentration  $[P]$  appearing in the model Eq. (1) was obtained by solving the system of differential Eqs. (2)–(5), using the LSODE method of numerical integration [23, 26]. The absolute precision (local truncation error) of the LSODE solver was set to  $10^{-15}$   $\mu\text{M}$ ; the relative precision was  $10^{-8}$  (eight significant digits) [23, 27].

$$d[E]/dt = -k_1[E][S] + k_2[ES] + k_3[ES] \quad (2)$$

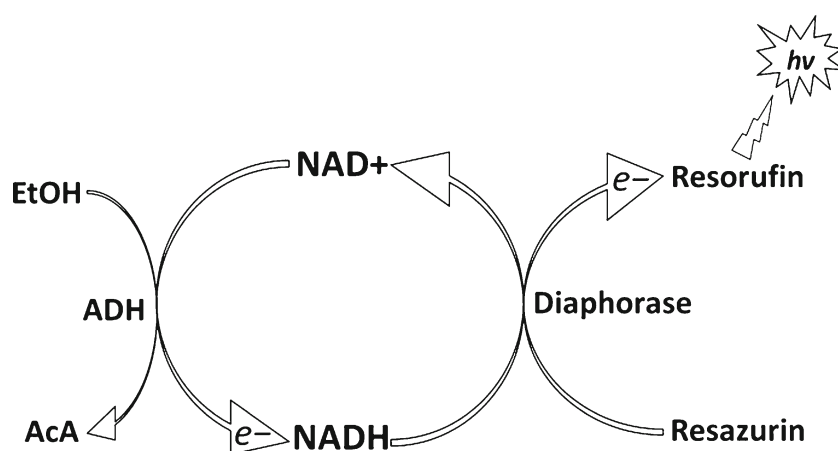
$$d[S]/dt = -k_1[E][S] + k_2[ES] \quad (3)$$

$$d[ES]/dt = +k_1[E][S] - k_2[ES] - k_3[ES] \quad (4)$$

$$d[P]/dt = +k_3[ES] \quad (5)$$

In the complete regression model represented by Eqs. (1)–(5), the adjustable model parameters were  $F_0$ ,  $r_p$ , and  $k_2$ . The bimolecular association rate constant  $k_1$  was held constant at  $10^8 \text{ M}^{-1} \text{ s}^{-1}$ ; the rate constant  $k_3$  were held fixed at

**Fig. 1** Schematic representation of the NAD cycling assay [13, 16]. Alcohol dehydrogenase oxidizes ethanol (EtOH) transferring electron to  $\text{NAD}^+$  and thus reducing it to NADH. On the other hand, diaphorase oxidizes NADH back to  $\text{NAD}^+$  transferring electron to resazurin which affords resorufin, a highly fluorescent end product of the reaction



$1 \text{ s}^{-1}$ . Initial reaction rates of resorufin formation (fluorescence units per second) were extracted from the numerical solution as  $r_p d[P]/dt$  at  $t=1 \text{ s}$ . Preliminary numerical simulations (results not shown) confirmed that the model system exists at quasi-steady-state approximately between  $t=0.1 \text{ s}$  and  $t=10 \text{ s}$ .

**Nonlinear Fit of Initial Rates** To obtain the parameters of a suitable nonlinear calibration curve, observed initial rates of resorufin formation (fluorescence units per second),  $v$ , in dependence on the  $\text{NAD}^+$  co-substrate concentration ( $[S]$ , nM) present in calibration samples were fit to the empirical regression model represented by Eq. (6) (for the DynaFit script see Supplement 3).

$$v = V_0 + V_{max} \frac{[S]/K_m + \beta[S]^2/K_m K_{ss}}{1 + [S]/K_m + [S]^2/K_m K_{ss}} \quad (6)$$

In Eq. (6),  $K_m$  is a Michaelis constant. The empirical parameters  $\beta$  and  $K_{ss}$  formally correspond to substrate inhibition ( $\beta < 1$ ) or substrate activation ( $\beta > 1$ ).

It is essential to ensure that the nonlinear calibration curve defined by Eq. (6) is strictly non-decreasing over the entire calibration range. Thus we require that  $dv/d[S] > 0$  in the range from  $[S] = 0$  to  $[S] = S_{max}$ . To ensure this monotonicity, our algorithm routinely checks that the inequality Eq. (7) holds for all calibration curves. In Eq. (7),  $N$  and  $D$  are auxiliary expressions defined by Eqs. (8) and (9), respectively;  $S_{max}$  is the maximum standard concentration of  $\text{NAD}^+$  (typically  $1 \text{ }\mu\text{M}$ ).

$$0 < 1 + 2\beta \frac{S_{max}}{K_{ss}} - \left(1 + 2\frac{S_{max}}{K_{ss}}\right) \frac{N}{D} \quad (7)$$

$$N = \frac{S_{max}}{K_m} \left(1 + \beta \frac{S_{max}}{K_{ss}}\right) \quad (8)$$

$$D = 1 + \frac{S_{max}}{K_m} \left(1 + \frac{S_{max}}{K_{ss}}\right) \quad (9)$$

If on any given plate the inequality (7) were not satisfied, our data-processing algorithm would automatically reject the entire plate as grossly defective. However, this particular anomalous condition was never encountered in practice.

The experimental design for the construction of the nonlinear calibration curve included 11 data points in duplicate (22 data points total). A 1:2 dilution series started from  $1000 \text{ nM}$   $\text{NAD}^+$ . Thus, the corresponding  $\text{NAD}^+$  concentrations were  $[S] = 1000, 500, \dots, 1.96, 0.98 \text{ nM}$ .

**Determination of  $\text{NAD}^+$ ,  $\text{NADH}$ , or Total  $\text{NAD}$**  For each unknown sample, the initial rate of resorufin formation was

measured in duplicates, using the method described above. The corresponding concentration of  $\text{NAD}^+$ ,  $S$ , was computed by using Eq. (10), where  $T$  and  $v'$  are auxiliary variables defined by Eqs. (11) and (12), respectively. In Eqs. (10)–(12),  $V_0$ ,  $V_{max}$ ,  $K_m$ ,  $K_{ss}$  and  $\beta$  are empirical parameters defining the nonlinear calibration curve.

$$S = \frac{\sqrt{T - K_{ss} V_{max}} + v' K_{ss}}{2v'} \quad (10)$$

$$T = K_{ss}^2 (V_{max} - v')^2 + 4v' K_m K_{ss} (\beta V_{max} - v') \quad (11)$$

$$v' = v - V_0 \quad (12)$$

## Results

**Initial Rates of Resorufin Formation** The reaction progress curves (i.e. fluorescence readings observed over time) in the cycling assay were nonlinear. A representative bow-shaped progress curve, shown in Fig. 2, was obtained at  $\text{NAD}^+$  concentration  $[S] = 3.91 \text{ nM}$ . The smooth continuous curve in Fig. 2 was obtained by iteratively reweighted least-squares fit (Huber's Mini-Max method [24]) to the system of Eqs. (1)–(5). The best-fit values of adjustable model parameters were  $k_2 = (1253 \pm 190) \text{ s}^{-1}$ ;  $r_p = (0.785 \pm 0.007) \times 10^6 \text{ RFU}/\mu\text{M}$ ; and  $F_0 = (0.0195 \pm 0.0009) \times 10^6 \text{ RFU}$ .

The inset in Fig. 2 shows that the instantaneous rate was constant (quasi steady-state) up to approximately  $t=10 \text{ s}$ . The observed initial rate of resorufin formation ( $62.2 \text{ RFU}/\text{sec}$ ) was extracted from the model curve at reaction time  $t=1 \text{ s}$ .

**Nonlinear Calibration Curve** Figure 3 shows the dependence of the observed initial rates of resorufin formation on the  $\text{NAD}^+$  concentration in the calibration wells. The experimental data in Fig. 3 (triangles) were fit to the empirical regression model represented by Eq. (6). The best-fit values of adjustable model parameters were  $V_0 = (0.001 \pm 0.003) \times 10^6 \text{ RFU}/\text{sec}$ ;  $K_m = (69 \pm 9) \text{ nM}$ ;  $K_{ss} = (820 \pm 300) \text{ nM}$ ;  $V_{max} = (1.1 \pm 0.1) \times 10^6 \text{ RFU}/\text{sec}$ ; and  $\beta = (1.17 \pm 0.08)$ . These best-fit values of model parameters define a nonlinear calibration curve, which is strongly nonlinear. The best-fit value of  $V_0 = 0.001 \times 10^6 \text{ RFU}/\text{sec}$  is effectively indistinguishable from zero given the best-fit value of  $V_{max} = 1.1 \times 10^6 \text{ RFU}/\text{sec}$ .

The inset in Fig. 3 shows the experimental data and the best-fit theoretical model in double logarithmic coordinates (logarithm of initial rate vs logarithm of standard  $\text{NAD}^+$  concentration). The logarithmic calibration curve is smooth

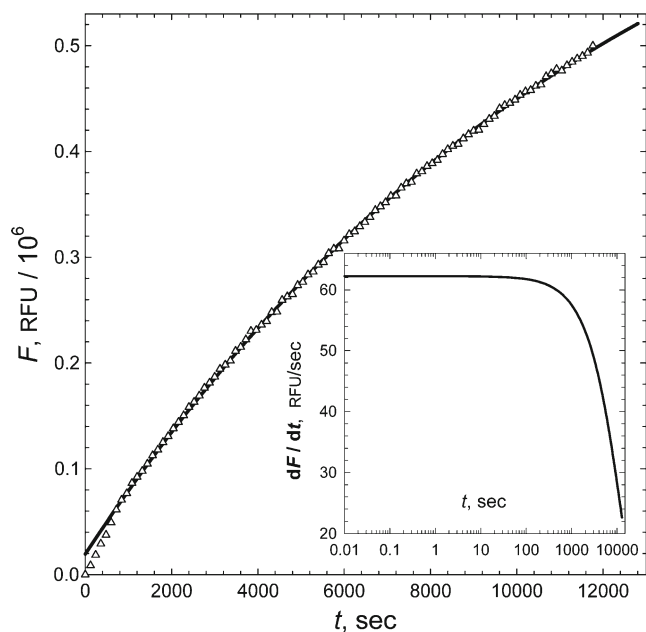


**Fig. 2** A representative progress curve from the cycling assay, used for construction of the calibration curve. *Triangles*: Experimental readings of fluorescence (relative fluorescence units, RFU). *Smooth curve*: Best-fit model generated from Eqs. (1) to (5); for details see text. Inset: Instantaneous rate plot corresponding to the model curve in the main panel

and regularly shaped over three orders of magnitude on the concentration axis (from 1 nM to 1  $\mu$ M standard  $\text{NAD}^+$ ).

**Determination of  $\text{NAD}^+$ ,  $\text{NADH}$ , or Total  $\text{NAD}$**  Each series of nucleotide determinations utilized a 96-well plate pipetted simultaneously with 22 standard samples (11  $\text{NAD}^+$  concentrations in duplicate) and with 72 unknown samples of cell lysates (36 unique samples in duplicates).

The determination of nucleotide contents in cell lysates proceeded in three stages. In the first stage all progress curves on the given plate were fit to the system of Eq. (1)–(5), to determine the initial rates of resorufin formation. In the second stage, the 24 initial rates for standard samples were fit to Eq. (6) to define the nonlinear calibration curve in terms of the calibration parameters  $V_0$ ,  $K_m$ ,  $K_{ss}$ ,  $V_{max}$ , and  $\beta$ . In the third and final stage, nucleotide content in the unknown samples were computed by using Eq. (10), utilizing the calibration parameters characteristic for the given plate.

An illustrative example is shown in Fig. 4. As part of a comprehensive optimization of the cycling assay, we performed cell lysis at specific time points (from 10 min to 20 h) after the last change of the growth medium. On the vertical axis we show the nucleotide contents from duplicate measurements separately for  $\text{NAD}^+$ ,  $\text{NADH}$ , and total  $\text{NAD}$  plotted against the time of lysis. The error bars attached to each data point in Fig. 4 show the standard deviation from quadruplicates. For better reproducibility and in order to be able to

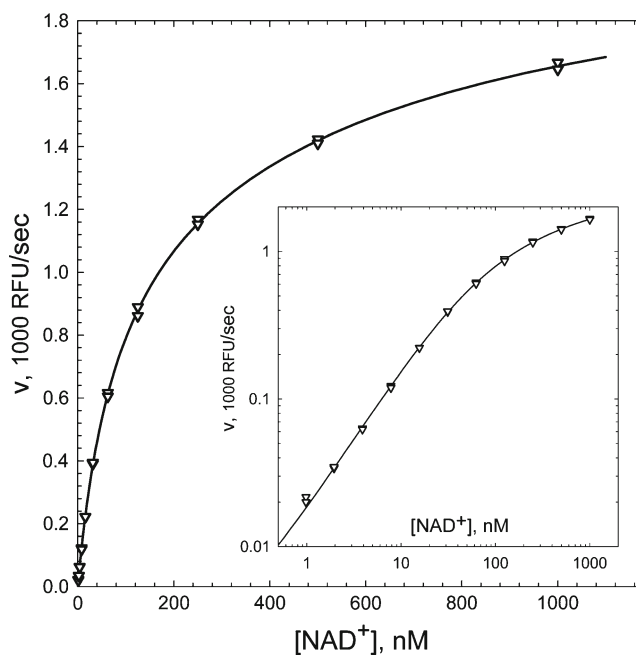


**Fig. 3** Nonlinear fit of observed initial rates in the cycling reaction. *Triangles*: Duplicated experimental initial rates (relative fluorescence units, RFU per minute) obtained by nonlinear fit of reaction progress curves (see for example Fig. 2). *Smooth curve*: Theoretical model curve obtained as the best fit to Eq. (6). For best-fit values of model parameters see text. Inset: The experimental and theoretical model plotted in logarithmic coordinates

compare data between various experiments, we normalized the  $\text{NAD}$  values to the total protein content in cell lysates.

The standard deviation from duplicates was minimal for all  $\text{NAD}^+$  or  $\text{NADH}$  measurements, such that the error bars drawn on the closed diamonds and triangles in Fig. 4 are essentially invisible. In contrast, the standard deviation from duplicates was at most ten percent for total  $\text{NAD}$  measurements (filled squares in Fig. 4). This shows that the nonlinear fitting method can ensure high accuracy/fidelity of data processing beyond linear ranges.

The accuracy of the determination was assessed by comparing the sum of  $\text{NAD}^+$  content and  $\text{NADH}$  content at any given time point (closed circles) with the total  $\text{NAD}$  content at the same cultivation time. We emphasize for clarity that these three types of measurements were performed independently from each other. For the 42 independent nucleotide determinations shown in Fig. 4 (21 data points in duplicate) the maximum relative deviation between  $[\text{NAD}^+] + [\text{NADH}]$  and total  $[\text{NAD}]$  was less than 9%. This further verified that both biochemical assay and data processing algorithms delivered satisfactory results outside the linear ranges.

**Comparison with Capillary Electrophoresis** Further validation of the proposed data-analytic approach is shown in Table 1, which compares the results from the cycling assay with the corresponding results provided by capillary electrophoresis

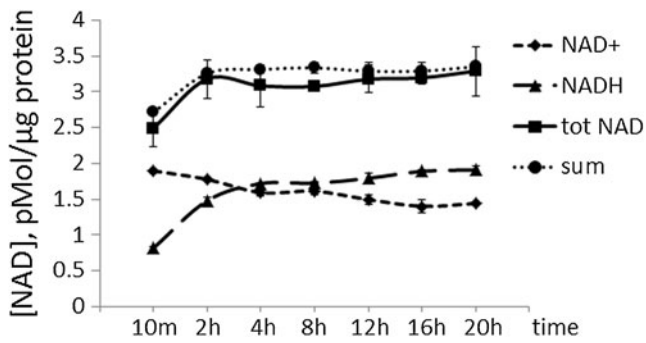


**Fig. 4** NAD nucleotide contents in cellular lysates of hESCs in response to addition of fresh medium. The cells in monolayers on Matrigel were grown in 12× plates; the medium was changed, and the cells were lysed when the indicated period of time elapsed. The NAD content was normalized towards the total protein content. The sum of NAD<sup>+</sup> plus NADH is compared to the total NAD content determined independently

(CE). The results show satisfactory agreement between analytical methods of different physical nature and different extraction and sample preparation methods employed.

**NAD Content in hESCs Under Various Physiologic Conditions** To further verify applicability of the optimized NAD assay to stem cells, we determined the NAD parameters in hESCs treated with FK866, a potent and specific inhibitor of nicotinamide phosphoribosyltransferase, which is a key enzyme in the NAD rescue pathway in mammalian cells [28]. Treatment with FK866 led to a depletion of the cellular NAD content (Fig. 5), in full agreement with the expected mode of action of the inhibitor [29]. We also additionally confirmed the phenomenon shown on Fig. 4, that the NAD content is a dynamic parameter which undergoes alterations after each change of the growth medium.

To apply the developed method for studying physiology of stem cells, we determined the NAD<sup>+</sup>, NADH and total NAD in different hESC lines, and compared them to the hESC-derived fibroblasts, differentiated from the same hESC line (Fig. 6). Our data show that the total NAD in hESCs lies around 3–3.5 pMol/μg of protein, while in the hESC-derived fibroblasts it is slightly higher, around 4–4.5-pMol/μg of protein. The total NAD values show tendency to increase during cultivation time (Fig. 6a). In contrast, the

**Table 1** Comparison of capillary electrophoresis (CE) and cycling assay results

Method	10 <sup>-18</sup> mol/cell	
	NAD <sup>+</sup>	NADH
CE	232±21 (n=11)	N. D.
NAD cycling assay	274±22 (n=20)	75±6 (n=20)

ratio of NAD<sup>+</sup> to NADH is more dynamic as a function of the time in culture, and differs dramatically from hESCs to hESC-derived fibroblasts where it is higher (Fig. 6b). Moreover, the ratio decreases during time in culture in both the stem cells and the hESC-derived fibroblasts. The NAD<sup>+</sup>/NADH ratio has been already shown as an important physiological parameter [7, 30]. Our data further point out that this metabolic ratio can be used for characterization of the functional status of the cells, e.g. their stemness.

Taken together, these suggest that both our biochemical assay and data processing algorithms can be used to study physiology of stem cells under various physiologic conditions.

## Discussion

Our conclusions are based on the following observations: (1) non-linearity is an intrinsic feature of the biochemical processes; (2) non-linear analytical reactions display reliably reproducible behavior outside of the (pseudo)linear range; (3) mechanism-based mathematical models of the reactions can reliably predict non-linear behavior of the analytical methods; (4) intrinsically non-linear biochemical reactions can be used for analytical purposes without forcing them into pseudo-linear ranges.

Two-enzyme cycling/chemical amplification systems have been in use for decades [15]. However, the overall utility of the experimental method has been limited by serious data-analytical challenges. The main difficulty lies in the fact that the experimental data are intrinsically nonlinear, whereas biochemical data analysts have been striving, traditionally, for linear regression models, which is an approximation by itself (see supplementary Fig. S1). Therefore, the accuracy and precision of the biological assays could only be achieved by

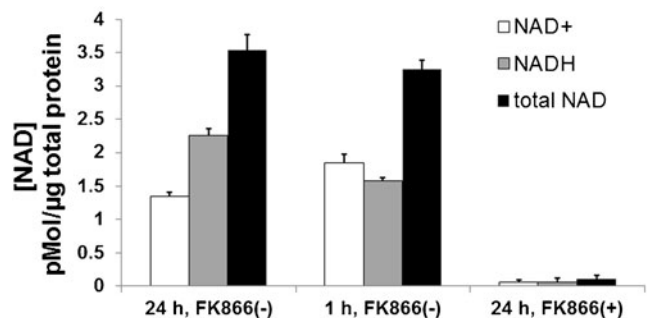


**Fig. 5** Cellular NAD nucleotide contents in hESCs under various physiological conditions. The hESCs were in fresh medium for 1 h after the routine change of standard growth medium without additives, compared with the cells in 24 h medium. 10 nM of FK866 was applied to cells for 24 h. Please note that all NAD values are dramatically diminished as a result of inhibition of the NAD rescue pathway. Cells were still viable, and their ATP content was still relatively high at this time point (not shown)

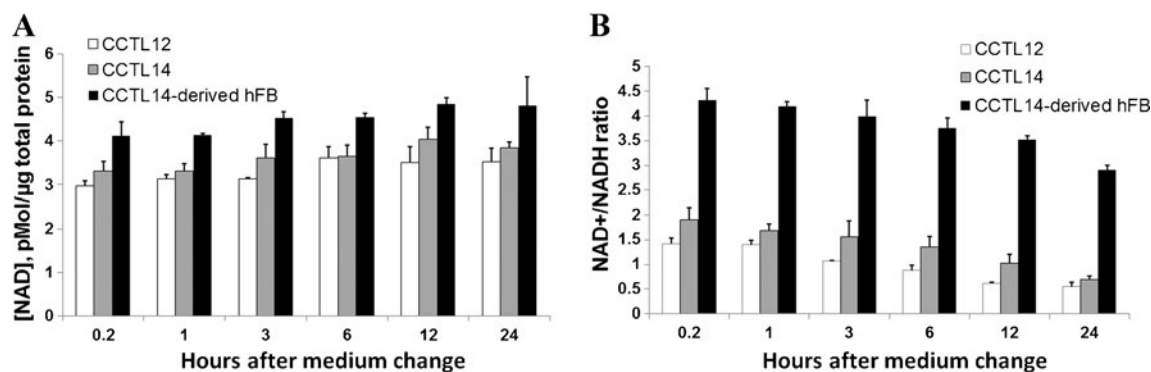


**Fig. 6** Cellular NAD nucleotide content in different hESC lines (CCTL12 and CCTL14) in comparison to hESC-derived fibroblasts (hFB) differentiated from the same hESC line. **a**, the cells grown in

monolayers were incubated in fresh standard medium for the time indicated, the total cellular NAD content is shown. **b**, cells were treated as in **a**, the ratio  $\text{NAD}^+/\text{NADH}$  is shown

using the non-linear regression models without severely compromising the dynamic range of the analytical reactions.

For example, Graef et al. [13] reported a cycling assay for nicotinic acid adenine dinucleotide phosphate (NAADP) with nanomolar sensitivity. Following the traditional approach, the authors analyzed their reaction progress curves using the straight-line fit. However, the authors show that the increase in resorufin fluorescence over time is decidedly nonlinear (see Fig. 1a in ref. [13]). Figure 1b in ref. [13] shows that the dependence of the initial rate on [NAAD] is also nonlinear. Similarly, Catomeris et al. [31] reported an intrinsically nonlinear calibration curve (see Fig. 6 in that report).

In the case of the reaction progress (i.e. the changes of resorufin fluorescence over time) the nonlinearity in the raw experimental data is fully expected e.g. simply on account of substrate depletion.

In the case of the calibration curves (i.e. the rate of fluorescence change vs known nucleotide concentration), the full kinetic model involving both cycling enzymes does predict that the calibration curves ([NAD] vs. initial rate) should be linear. This prediction was confirmed by numerical simulations of the full two-enzyme mechanism using the complete system of differential equations (results not shown). We do not fully understand why the calibration curves, such as for example the calibration curve shown in Fig. 3, are nonlinear. One plausible hypothesis is the fluorescence inner filter effect, which is very pronounced in the resazurin/resorufin detection system [31]. Another possibility is that the two-enzyme system displays substrate- or product-inhibition effects.

Whatever the reasons for nonlinearity, rather than to “force” linear regression onto experimental data that are clearly nonlinear, here we propose a data-analytic approach where the intrinsic nonlinearity of the experimental data is matched with the nonlinearity of the fitting model. The overall data-analytic protocol allowed us to determine nucleotide amounts in cell lysates that span from single digit nanomolar to micromolar, representing three orders of magnitude. We verified the accuracy of our biochemical setup and data processing by a comparison

between  $[\text{NAD}^+] + [\text{NADH}]$  and total [NAD] from independent determinations (Fig. 4). To further verify our assay, we determined the NAD content in cells treated with FK866, a specific inhibitor of the NAD rescue pathway, which can reduce the NAD levels to sub-physiological levels [28, 29]. We thus showed that our method can reliably and reproducibly detect the changes in the intracellular NAD levels (Fig. 5).

Using our approaches we determined the amount of NAD in human embryonic stem cells in a resting monolayer culture (Table 1). To the best of our knowledge, this is the first account for the  $\text{NAD}^+$ , NADH and total NAD content in hESCs. The reported values are in a good agreement with previously reported data for eukaryotic cells [32]. In addition, using our methodology we were able to show that the cellular NAD parameters undergo alterations upon routine changes of culture medium (Figs. 4, 5 and 6). Importantly, the  $\text{NAD}^+/\text{NADH}$  ratio was found to be substantially higher in hESC-derived fibroblasts in comparison to stem cell lines. This suggests that the  $\text{NAD}^+/\text{NADH}$  ratio can be used for characterization of the functional status of the various cell types, e.g. cell stemness. The higher ratio in fibroblasts points out that their mitochondria efficiently utilize the NADH in oxidative phosphorylation, as compared to the stem cells. In addition, the total NAD levels are also higher in fibroblasts in comparison to the stem cells, although the difference is not as prominent as in the case of the  $\text{NAD}^+/\text{NADH}$  ratio. This further suggests that the set of metabolic parameters, including the NAD values, could be used to characterize the ability of cell to self-renew and to differentiate.

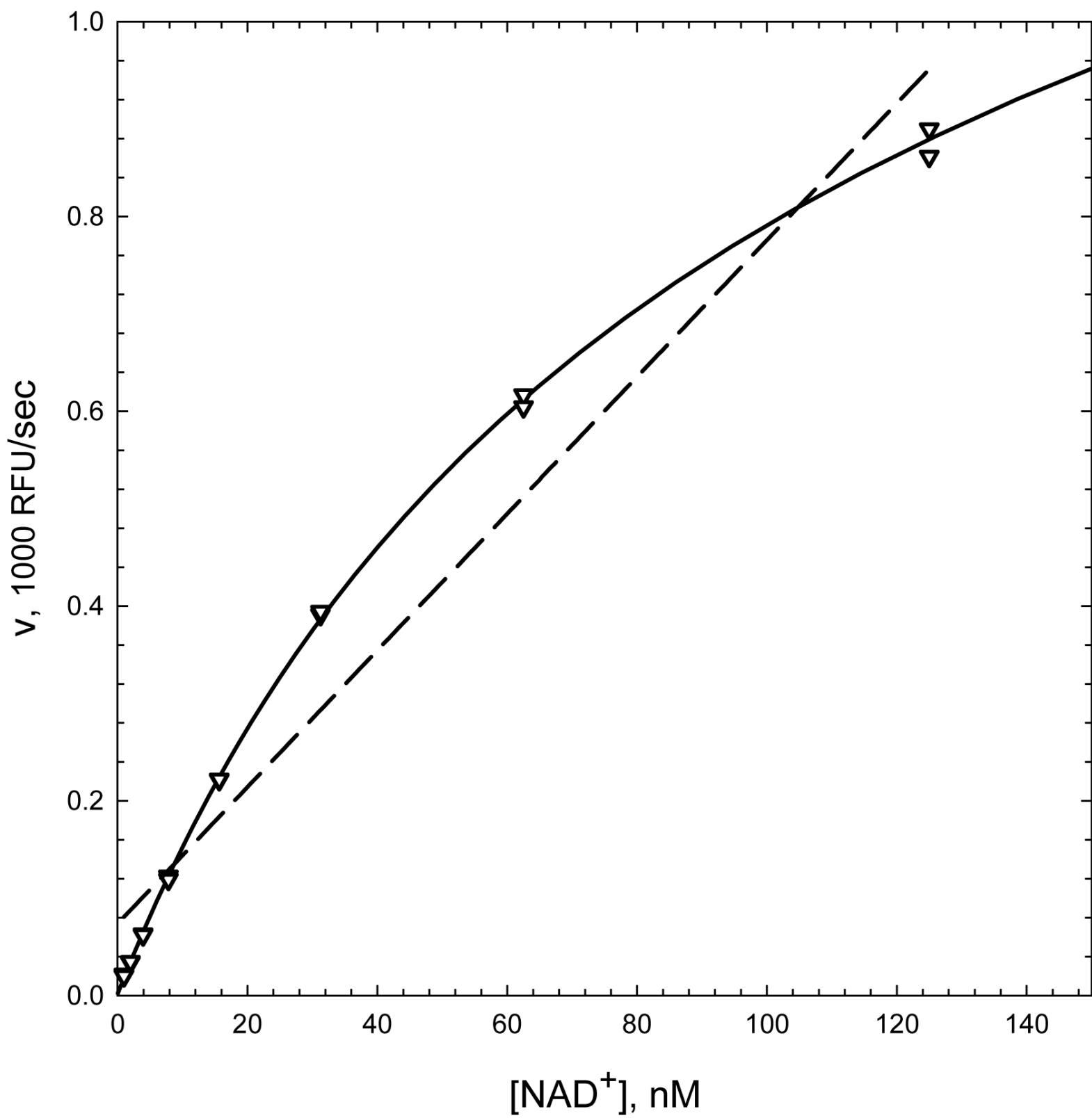
**Acknowledgments** We acknowledge support from the Ministry of Education, Youth, and Sport of the Czech Republic (MSMT0021622430). This work also received a financial contribution from the European Community within the Seventh Framework Programme (FP/2007-2013) under Grant Agreement No. 229603 co-financed by the South Moravian Region of Czech Republic within the SoMoPro programme [to SK], and was supported by European Regional Development Fund - Project FNUSA-ICRC (No.CZ.1.05/1.1.00/02.0123) [to AS] and from Czech Science Foundation grant GAP206/11/0009 [to JM]. We thank Dr. Rotrekl for providing hESC-derived fibroblasts and National Institute of Mental

Health's (NIMH) Chemical synthesis and drug supply program, USA for FK866.

**Conflict of Interest** All authors declare no conflict of interest.

## References

- Folmes, C. D., Nelson, T. J., Dzeja, P. P., & Terzic, A. (2012). Energy metabolism plasticity enables stemness programs. *Annals of the New York Academy of Sciences*, *1254*, 82–89.
- Kondoh, H., Leonart, M. E., Nakashima, Y., et al. (2007). A high glycolytic flux supports the proliferative potential of murine embryonic stem cells. *Antioxidants Redox Signal*, *9*, 293–299.
- Folmes, C. D., Dzeja, P. P., Nelson, T. J., & Terzic, A. (2012). Metabolic plasticity in stem cell homeostasis and differentiation. *Cell Stem Cell*, *11*, 596–606.
- Araki, T., Sasaki, Y., & Milbrandt, J. (2004). Increased nuclear NAD biosynthesis and SIRT1 activation prevent axonal degeneration. *Science*, *305*, 1010–1013.
- Hinz, M., Katsilambros, N., Maier, V., Schatz, H., & Pfeiffer, E. F. (1973). Significance of streptozotocin induced nicotinamide-adenine-dinucleotide (NAD) degradation in mouse pancreatic islets. *FEBS Letters*, *30*, 225–228.
- Benavente, C., Jacobson, M., & Jacobson, E. (2009). NAD in skin: therapeutic approaches for niacin. *Current Pharmaceutical Design*, *15*, 29–38.
- Lin, S.-J., & Guarente, L. (2003). Nicotinamide adenine dinucleotide, a metabolic regulator of transcription, longevity and disease. *Current Opinion in Cell Biology*, *15*, 241–246.
- Soane, L., Kahraman, S., Kristian, T., & Fiskum, G. (2007). Mechanisms of impaired mitochondrial energy metabolism in acute and chronic neurodegenerative disorders. *Journal of Neuroscience Research*, *85*, 3407–3415.
- Wang, J., Zhai, Q., Chen, Y., et al. (2005). A local mechanism mediates NAD-dependent protection of axon degeneration. *The Journal of Cell Biology*, *170*, 349–355.
- Yang, H., Yang, T., Baur, J. A., et al. (2007). Nutrient-sensitive mitochondrial NAD<sup>+</sup> levels dictate cell survival. *Cell*, *130*, 1095–1107.
- Biason-Lauber, A., Böni-Schnetzler, M., Hubbard, B. P., et al. (2013). Identification of a SIRT1 mutation in a family with type 1 diabetes. *Cell Metabolism*, *17*, 448–455.
- Dilgin, D. G., Gligor, D., Gökçel, H. İ., Dursun, Z., & Dilgin, Y. (2010). Photoelectrocatalytic oxidation of NADH in a flow injection analysis system using a poly-hematoxylin modified glassy carbon electrode. *Biosensors and Bioelectronics*, *26*, 411–417.
- Graeff, R., & Lee, H. C. (2002). A novel cycling assay for nicotinic acid-adenine dinucleotide phosphate with nanomolar sensitivity. *Biochemical Journal*, *367*, 163–168.
- Emancipator, K., & Kroll, M. H. (1993). A quantitative measure of nonlinearity. *Clinical Chemistry*, *39*, 766–772.
- Lowry, O. H., Passonneau, J. V., Schulz, D. W., & Rock, M. K. (1961). The measurement of pyridine nucleotides by enzymatic cycling. *Journal of Biological Chemistry*, *236*, 2746–2755.
- Lowry, O. H. (1980). Amplification by enzymatic cycling. *Molecular and Cellular Biochemistry*, *32*, 135–146.
- Dvorak, P., Dvorakova, D., Koskova, S., et al. (2005). Expression and potential role of fibroblast growth factor 2 and its receptors in human embryonic stem cells. *Stem Cells*, *23*, 1200–1211.
- Kunova, M., Matulka, K., Eiselleova, L. et al. (2013). Adaptation to robust monolayer expansion produces human pluripotent stem cells with improved viability. *Stem Cells Translational Medicine*, *2*, 246–254.
- Krutá, M., Bálek, L., Hejnová, R., et al. (2012). Decrease in abundance of apurinic/aprimidinic endonuclease causes failure of base excision repair in culture-adapted human embryonic stem cells. *Stem Cells*, *31*, 693–702.
- Bubis, M., & Zisapel, N. (1998). A role for NAD<sup>+</sup> and cADP-ribose in melatonin signal transduction. *Molecular and Cellular Endocrinology*, *137*, 59–67.
- Lin, S. S., Manchester, J. K., & Gordon, J. I. (2001). Enhanced gluconeogenesis and increased energy storage as hallmarks of aging in *Saccharomyces cerevisiae*. *Journal of Biological Chemistry*, *276*, 36000–36007.
- Musilova, J., Sedlacek, V., Kucera, I., & Glatz, Z. (2009). Capillary zone electrophoresis with field enhanced sample stacking as a tool for targeted metabolome analysis of adenine nucleotides and co-enzymes in *Paracoccus denitrificans*. *Journal of Separation Science*, *32*, 2416–2420.
- Kuzmic, P. (1996). Program DYNAFIT for the analysis of enzyme kinetic data: application to HIV proteinase. *Analytical Biochemistry*, *237*, 260–273.
- Huber, P. J. (1981). *Robust statistics*. New York: John Wiley & Sons.
- Rousseeuw, P. J., & Leroy, A. M. (1987). *Robust regression and outlier detection*. New York: Wiley-Interscience.
- Hindmarsh, A. C. (1983). ODEPACK: A systematized collection of ODE solvers. In R. S. Stepleman (Ed.), *Scientific computing* (pp. 55–64). Amsterdam: North Holland.
- Kuzmič P. (2009). DynaFit—A software package for enzymology. *467*, 247–280.
- Hasmann, M., & Schemainda, I. (2003). FK866, a highly specific noncompetitive inhibitor of nicotinamide phosphoribosyltransferase, represents a novel mechanism for induction of tumor cell apoptosis. *Cancer Research*, *63*, 7436–7442.
- Holen, K., Saltz, L. B., Hollywood, E., Burk, K., & Hanauske, A.-R. (2008). The pharmacokinetics, toxicities, and biologic effects of FK866, a nicotinamide adenine dinucleotide biosynthesis inhibitor. *Investigational New Drugs*, *26*, 45–51.
- Wellen, K. E., & Thompson, C. B. (2012). A two-way street: reciprocal regulation of metabolism and signalling. *Nature Reviews Molecular Cell Biology*, *13*, 270–276.
- Catomeris, P., & Thibert, R. J. (1988). Study and optimization of the resazurin/diaphorase system. *Microchemical Journal*, *38*, 390–398.
- Xie, W., Xu, A., & Yeung, E. S. (2009). Determination of NAD(+) and NADH in a single cell under hydrogen peroxide stress by capillary electrophoresis. *Analytical Chemistry*, *81*, 1280–1284.



## Supplement 2.

```
;

---

  
[task]  
    data = progress  
    task = fit  
    model = FILE  
[mechanism]  
    E + S <==> ES : kas kds  
    ES ---> E + P : kdp  
[constants]  
    kas = 100  
    kds = 1000 ?  
    kdp = 0.01 ?  
[concentrations]  
    E = 0.01  
    S = 1  
[responses]  
    P = 1000 ?  
[settings]  
{Filter}  
    TimeMin = 600  
    TimeInitialRate = 5  
[output]  
    directory OUTPUTDIR  
; REPEAT TASK  
[data]  
    directory DATADIR  
    extension txt  
    file FILE | offset 0 ?  
[end]  
  
;

---


```

*DynaFit Script 1.* Fitting reaction progress curves (time  $t$  vs fluorescence  $F$ ) to Eq. (1) by using Huber's Mini-Max method for robust regression analysis. The first 5 time points were excluded from the data analysis, assuming that this time is enough for both temperature stabilizing and mixing of the reaction environment. For more details see explanation in the text.

### Supplement 3.

```
;

---

  
[task]  
    task = fit  
    data = generic  
[parameters]  
    Ks, Ks2, Vmax, Vmax2, Vo, S  
[model]  
    Ks    = 1000 ?  
    Ks2   = 10000 ?  
    Vmax  = 1 ?  
    Vmax2 = 0.1 ?  
    Vo    = 0.01 ?  
  
    num = Vmax*S/Ks + Vmax2*S*S/Ks/Ks2  
    den = 1 + S/Ks + S*S/Ks/Ks2  
    v   = Vo + num/den  
[data]  
    variable  S  
    file      ./RUNNAME/data/rates/nad.txt  
    plot      linear  
[output]  
    directory ./RUNNAME/output/fit-rates  
[settings]  
{Marquardt}  
    RobustFit = y  
[end]  
;
```

*DynaFit Script 2.* Fitting initial rates of resorufin formation (fluorescence units per second) to the empirical regression model represented by Eq. (6), in dependence on the NAD<sup>+</sup> concentration in calibration samples. For more details see explanation in the text.